npj | Computational Materials

www.nature.com/npjcompumats

REVIEW ARTICLE OPEN

Computationally predicted energies and properties of defects in GaN

John L. Lyons[1] and Chris G. Van de Walle[2]

Recent developments in theoretical techniques have significantly improved the predictive power of density-functional-based calculations. In this review, we discuss how such advancements have enabled improved understanding of native point defects in GaN. We review the methodologies for the calculation of point defects, and discuss how techniques for overcoming the band-gap problem of density functional theory affect native defect calculations. In particular, we examine to what extent calculations performed with semilocal functionals (such as the generalized gradient approximation), combined with correction schemes, can produce accurate results. The properties of vacancy, interstitial, and antisite defects in GaN are described, as well as their interaction with common impurities. We also connect the first-principles results to experimental observations, and discuss how native defects and their complexes impact the performance of nitride devices. Overall, we find that lower-cost functionals, such as the generalized gradient approximation, combined with band-edge correction schemes can produce results that are qualitatively correct. However, important physics may be missed in some important cases, particularly for optical transitions and when carrier localization occurs.

npj Computational Materials (2017)3:12 ; doi:10.1038/s41524-017-0014-2

INTRODUCTION

The advent of III-nitrides as semiconductor materials has enabled the new technology of solid-state lighting[1] and opened new directions in established technologies such as solar cells,[2] and power electronics.[3] GaN and related materials such as InN, AlN, and BN are also being investigated for applications in photocatalysis[4] and thermoelectrics.[5] In each of these applications, the presence of native defects (see Fig. 1) can strongly affect device performance. Such defects can play a beneficial role, for instance acting as reaction centers in photocatalytic materials[4] or as candidate qubits for quantum information science.[6] More often their presence has a detrimental effect, such as nonradiative recombination in light emitters.[7, 8]

Detrimental defect behavior is most often caused by localized states in the semiconductor band gap, which can affect device efficiency due to nonradiative recombination, carrier trapping and scattering, and parasitic luminescence or absorption. The presence of such "deep" states due to native defects in GaN has long been known experimentally.[9] First-principles calculations soon followed.[10–14]

These calculations were performed using density functional theory (DFT),[15, 16] which since its inception has provided a theoretical basis for determining the electronic structure of semiconductors and their surfaces, interfaces, and native defects. Such studies were instrumental in elucidating the electronic character and chemical stability of native defects in the nitrides. However, DFT implemented with local or semilocal functionals such as the local density approximation (LDA)[16–18] or generalized gradient approximation (GGA)[19] cannot provide quantitative predictions of defect transition levels and formation energies. This failure results from a number of factors, including the well-known band-gap error, the inability to correctly describe carrier localization, and self-interaction errors. Significant progress was made with the introduction of hybrid functionals.[20] In addition, the early calculations suffered inaccuracies due to finite-size errors inherent in supercell calculations for charged defects. We will show that the intrinsic DFT errors and the finite-size errors fortuitously cancel for a number of important defects, rendering the early results more reliable than might have been expected.

We will review how the application of first-principles techniques has changed the understanding of native defect behavior in the nitride semiconductors. Other reviews have provided a detailed description of the formalism, thermodynamic basis, and theoretical underpinnings of defect calculations[12, 21, 22]; therefore these topics are discussed only briefly in computational approach. In Comparison between results obtained with different functionals, we describe the overall comparison between results obtained with different functionals. An important focus of the present work is an examination of the extent to which calculations performed with the GGA, combined with correction schemes, can produce accurate results (as benchmarked against a hybrid functional). Then, in the subsections of Native defects in GaN, we discuss in detail the results for each defect separately. We will see that even the most stable native defects have relatively large formation energies; therefore we also discuss how the properties of native defects are affected by the formation of complexes with common impurities. Throughout this review, we will provide a critical examination of results in the literature, and discuss connections to experiment and the implications for devices.

Computational approach

The calculation of defect formation energies and transition levels follows from a well established formalism[22]; for example, the

[1]Center for Computational Materials Science, Naval Research Laboratory, Washington, DC 20375, USA and [2]Materials Department, University of California, Santa Barbara, CA 93106-5050, USA
Correspondence: John L. Lyons (john.lyons@nrl.navy.mil)
John L. Lyons and Chris G. Van de Walle contributed equally to this work.

Received: 16 November 2016 Revised: 31 January 2017 Accepted: 13 February 2017
Published online: 24 March 2017

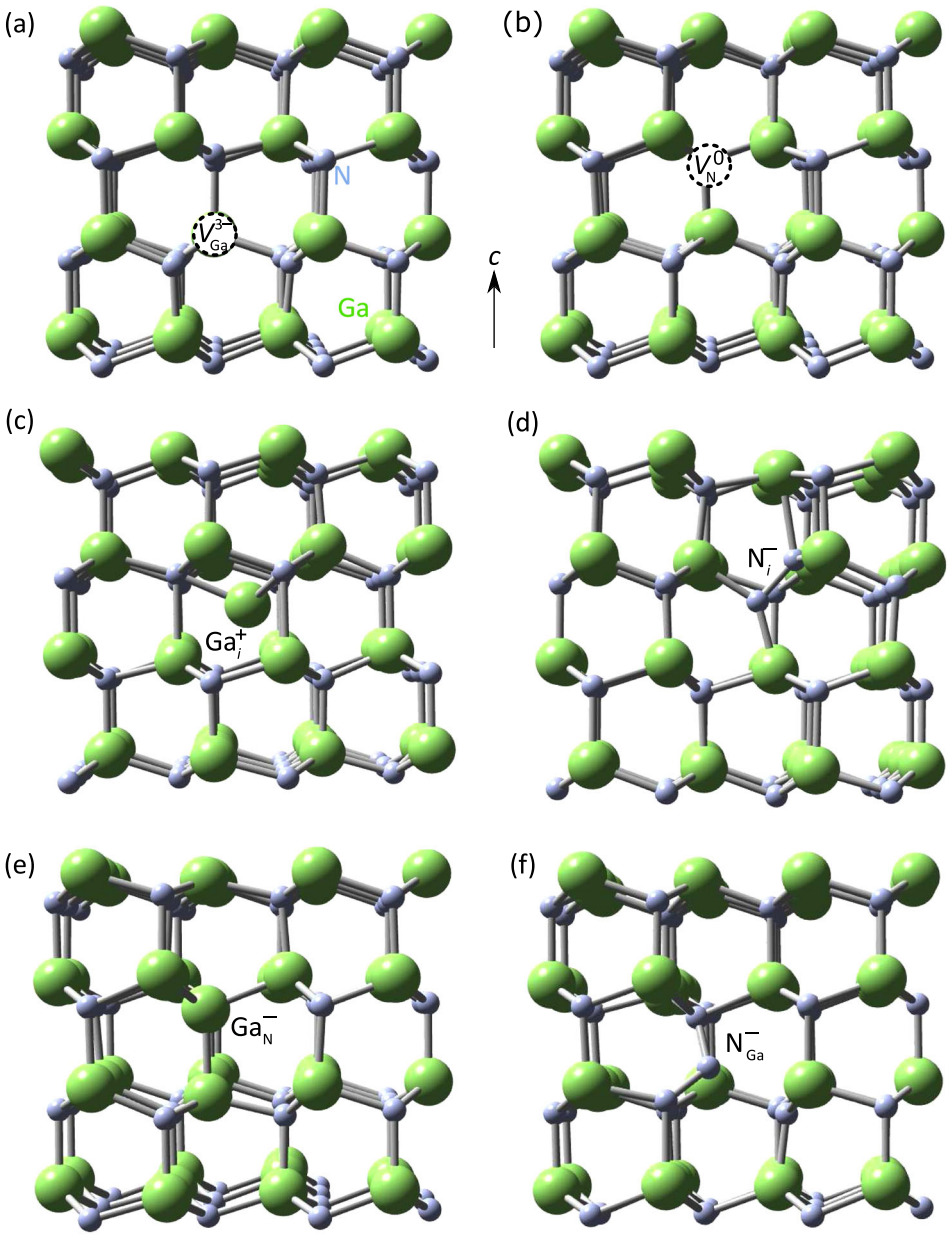

Fig. 1 Configurations of native defects in GaN. **a** V_{Ga}^{3-}, **b** V_N^0, **c** Ga_i^+, **d** N_i^-, **e** Ga_N^-, and **f** N_{Ga}^-, in the charge states that are stable in *n*-type GaN

formation energy of a gallium vacancy (V_{Ga}) in charge state q is given by:

$$E^f(V_{Ga}^q) = E_{tot}(V_{Ga}^q) - E_{tot}(GaN) + \mu_{Ga} + q(E_F + \varepsilon_v) + \Delta^q, \quad (1)$$

in which $E_{tot}(V_{Ga}^q)$ is the total energy of a supercell containing V_{Ga}^q in charge state q, and E_{tot} (GaN) is the total energy of the same supercell without a defect. Electrons added or removed from the supercell are exchanged with the Fermi level (E_F) of the semiconductor host which is referenced to the valence-band maximum (VBM) (ε_v).

Δ^q corresponds to a correction for the finite size of charged supercells. As discussed in refs. 22 and 23, a number of methods have been proposed for obtaining such corrections.[24, 25] The new results presented in this paper have been calculated using the procedure outlined in refs. 25 and 26, which is a a scheme based on the explicit treatment of the electrostatic problem. As shown in ref. 25, this approach is capable of providing more accurate corrections than Madelung-type approaches for moderately-sized supercells.

Here we also use 96-atom wurtzite supercells, 400 eV plane-wave cutoffs, special k-point meshes, Ga projector-augmented-wave potentials with 3*d* states in the core, and the projector-augmented wave (PAW)[27] method as implemented in VASP.[28] Spin polarization is explicitly included.

Most point defects can be stable in several different charge states, depending on the position of the Fermi level. As the Fermi level is raised, defect-induced states within the band gap become filled with electrons. What we commonly think of as "defect levels" correspond to Fermi-level positions where a transition from one charge state to another one occurs. Technically, these levels are defined as "thermodynamic transition levels", and they correspond to the Fermi-level positions where the formation energies of two charge states of a defect are equal. The transition level between charge states

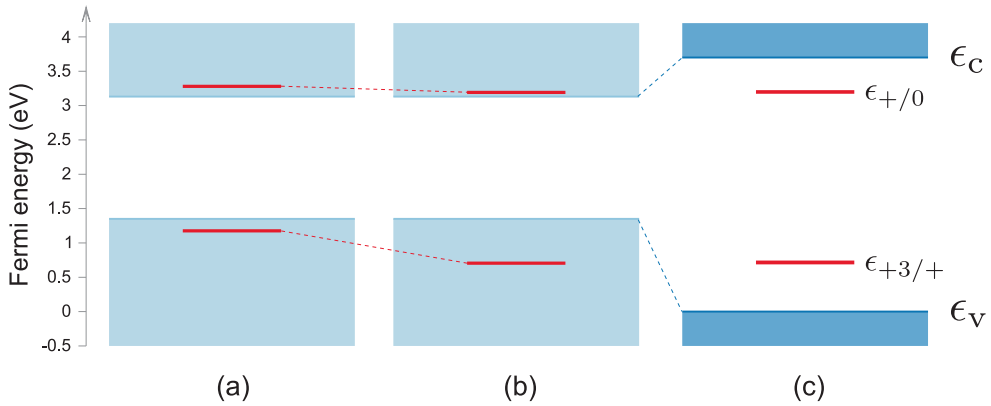

Fig. 2 Thermodynamic transition levels of V_N in GaN, calculated with the PBE functional **a** without and **b** with finite-size corrections. In **c**, the HSE-calculated band gap is used, and the PBE-calculated transition levels are positioned by aligning the band edges through the average electrostatic potentials. (Reprinted from Ref. 54 with permission from Elsevier)

q and q' is given as:

$$(q/q') = \frac{E^f(q; E_F = 0) - E^f(q'; E_F = 0)}{q' - q}, \quad (2)$$

where $E^f(q;\ E_F = 0)$ and $E^f(q';\ E_F = 0)$ represent the formation energies of the q and q' charge states when the Fermi level is at 0 eV (i.e., the VBM).

We will also discuss optical transitions that can occur due to recombination, i.e., capture of carriers from a band edge into a defect level. As outlined in ref. 29, such transitions can be described through the construction of a configuration-coordinate (CC) diagram, which describes how the energy of specific charge states depends on the changes in coordinates that occur when atomic relaxations are different for each of the charge states. Peak optical transition energies (either in absorption or emission processes) will then differ from the thermodynamic transition level by the Franck-Condon (FC) shift. In this work, the FC shift will be approximated by the energy difference between a charged defect in its equilibrium configuration and the same defect when placed in the equilibrium configuration of an excited charge state.

In this work, we will present results obtained with the GGA of Perdew, Burke, and Ernzenhof (PBE) and with the hybrid functional due to Heyd, Scuseria, and Ernzerhof (HSE).[30, 31] These functionals vary in their treatment of the exchange-correlation (XC) energy. GGAs such as PBE use a semilocal approximation of the XC energy through a functional of the density and its gradient. In contrast, hybrid functionals such as HSE approximate the XC energy by incorporating a fraction of exact Hartree-Fock exchange into the XC potential.

As mentioned in the introduction, semilocal functionals such as PBE do not give accurate band gaps. For example, as reported in ref. 32, within GGA-PBE the band gap of AlN is underestimated by 34%, the band gap of GaN is underestimated by 55%, and InN is predicted to be metallic. Band-gap errors of this magnitude clearly lead to uncertainties in defect transition levels and formation energies. In principle, quasiparticle calculations provide a more accurate description,[33, 34] but these are computationally intensive and are based on geometries that are obtained with DFT.[35, 36] Quantum Monte Carlo calculations[37–39] can also provide a direct solution to the many-body problem, but applications to defects have been limited due to the computational complexity.

Staying within DFT is desirable, but clearly the accuracy needs to be improved over that obtained with local or semilocal functionals. A variety of approaches have been proposed,[22] including applications of Hubbard-U-like terms (LDA + U or GGA + U) to cation d states[40] or to multiple orbital channels,[41] the Slater-Janak transition model,[42, 43] modified pseudopotentials,[44] Becke-Johnson type functionals,[45, 46] combining DFT with quasiparticle calculations,[35, 36] and hybrid functionals.[47–56] Hybrid functionals have emerged as the current method of choice,[22] applicable to a wide variety of systems including defects in Si,[47, 48] GaAs,[51] diamond,[48] and oxides.[49, 50] In the following, unless specified otherwise, we assume that hybrid functional results are obtained with HSE.[30, 31] Here, we set the fraction of exact exchange to 0.31 so that a band gap of 3.51 eV is obtained, in agreement with the experimental value.[57] The GaN lattice parameters are much less sensitive to the choice of functional. Both PBE ($a = 3.22$ Å, $c = 5.22$ Å) and HSE ($a = 3.19$ Å, $c = 5.17$ Å) produce values close to experiment ($a = 3.19$ Å, $c = 5.19$ Å).

Comparison between results obtained with different functionals

The adoption of the hybrid functional approach invites a comparison between results obtained with hybrid functionals vs. LDA or GGA. Such a comparison allows an assessment of the reliability of previously published work based on (semi)local functionals. In addition, it sheds light on whether low-cost GGA-based defect calculations can be sufficiently accurate for determining the suitability of materials through high-throughput screening techniques.[58]

Alkauskas, Broqvist, and Pasquarello identified that accounting for the band edge shifts was crucial for comparing defect results from different functionals.[59] For shallow defects (i.e., defects that do not give rise to thermodynamic transition levels within the semiconductor band gap), it was shown that formation energies calculated with GGA can be corrected by accounting for the shift in the band edges.[60] Indeed, the underestimation of the band gap in GGA means that the VBM typically lies too high on an absolute energy scale (e.g., referenced to the vacuum level), and the conduction-band minimum (CBM) lies too low. Correcting for the positions of these band edges by aligning the GGA and hybrid functional calculations to the vacuum level brought the GGA values for formation energies into agreement with HSE values to within 0.5 eV.[60]

Alkauskas and Pasquarello[50, 59] applied this concept to deep defects (i.e., those with transition levels within the semiconductor band gap), and aligned the GGA and hybrid functional band structures through an alignment of the average electrostatic potentials. Miceli and Pasquarello[54] applied this approach to point defects in GaN, i.e., they performed the defect calculations with PBE and then shifted the band edges based on HSE calculations (see Fig. 2). However, they did not explicitly compare their results with fully consistent hybrid functional calculations.

Freysoldt *et al.*[61] used a slightly different band-alignment strategy, based on aligning a benchmark defect level between GGA and hybrid functional calculations; they also included changes to reference energies for chemical potentials between functionals. This scheme produced agreement between LDA/GGA and HSE results to better than 0.2 eV for a set of point defects, impurities, and complexes that included hydrogen interstitials, Mg substitutional impurities, isolated V_N, and V_N-related complexes.

All these approaches presuppose that LDA/GGA calculations produce a reasonable description of atomic geometries and defect wavefunctions, i.e., that hybrid functional calculations will not significantly affect the defect behavior and that the major change occurs due to the shift in bulk band edges. This assumption will be scrutinized in the present paper. (The additional host chemical potential correction employed in ref. 61 is relatively small: less than 0.1 eV for μ_{Ga}. Such corrections will not be considered further in this paper.)

A recent study[62] compared LDA-calculated defect levels with results from a screened exchange LDA ("sx-LDA"[63]) functional that incorporates non-local Fock exchange into the LDA. This study found significant differences in defect transition levels, but did not consider band-edge alignment between LDA and sx-LDA.

In the following section we provide a direct comparison between the formation energies and transition levels of native defects in GaN calculated from GGA and HSE. In subsequent sections we further discuss how application of hybrid functionals has altered the understanding of each defect individually.

Formation energies of native defects in GaN calculated with GGA (PBE) and HSE are presented in Fig. 3. Ga-rich conditions [$\mu_{Ga} = \mu_{Ga_{bulk}}$ in Eq. (1)] have been chosen. A comparison between GGA and HSE results is enabled by performing an alignment of the GGA and HSE band structures. We determine this alignment by performing vacuum-slab calculations of the $(10\bar{1}0)$ non-polar surface, using 12 atomic layers and allowing the outer two bilayers to relax. Conducting these calculations separately with each functional provides an alignment of the VBMs with the vacuum level (further details are discussed in ref. 60). This results in a valence-band offset of 0.85 eV between the GGA and HSE valence bands of GaN. In Fig. 3, for the GGA results, we extended the range of the Fermi level below the VBM (at 0 eV) down to −0.85 eV to account for the valence-band offset with HSE. The Fermi level is also extended beyond the CBM, which occurs at 1.71 eV (the GGA band gap), in order to align with the HSE-calculated band gap of 3.51 eV.

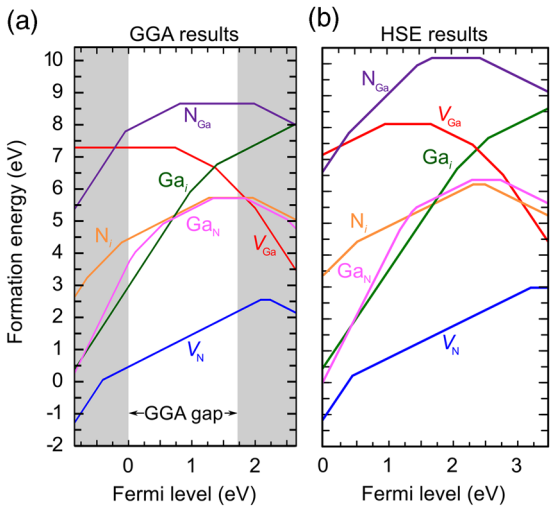

Fig. 3 Formation energies vs. Fermi level for interstitial, vacancy, and antisite defects in GaN, calculated with **a** GGA and **b** HSE hybrid functionals. Both sets of formation energies include finite-size corrections as described in the text. In **a**, the white region indicates the GGA-calculated band gap; the Fermi-level range is extended beyond the band maxima (*grey* regions) so that the edges of the plot correspond to the HSE range shown in **b**. In both cases, Ga-rich conditions are chosen

Our procedure for aligning GGA and HSE results is very similar to the approach of Miceli and Pasquarello[54] mentioned above, except that they obtained the alignment using the average electrostatic potential as a reference, whereas we use the vacuum level as a reference. Both approaches are approximations: in case of the electrostatic potential, one assumes that the bulk charge density is virtually unchanged between GGA and HSE; in case of vacuum alignment, one assumes that any surface dipoles are very similar in HSE and GGA. We have performed an explicit comparison between the two approaches: the electrostatic potential alignment yields an alignment of 0.77 eV between GGA and HSE valence bands, in good agreement with the 0.85 eV value obtained from vacuum alignment. Miceli and Pasquarello[54] reported a value of 1.4 eV for the valence-band offset (see Fig. 2), obtained from electrostatic-potential alignment. This disagreement is very puzzling, since their computational approach is otherwise very similar to the one in the present work. The difference explains why the defect levels calculated by Miceli and Pasquarello[54] generally appear higher in the band gap than the ones we will report below. We note, however, that the difference is not always as large as 0.55 eV (the difference in band alignments); e.g., for the (3+/+) transition level of V_N 0.68 eV was reported in ref. 54, while we find 0.45 eV. Another difference between our work and that of ref. 54 is that norm-conserving pseudopotentials were employed in the latter, while we use PAWs; however, our own tests indicate that this difference is not expected to lead to significant discrepancies.

Figure 3 shows that the results from GGA with the properly aligned and extended band gap (we will refer to this approach as "shifted GGA") and from HSE are remarkably similar. For each defect, the same set of charge-state transition levels are present (with the exception of the (+/0) level of V_{Ga}, which will be discussed in Gallium vacancies). The quantitative differences between the positions of charge-state transition levels will be discussed below. We observe that V_N is the most stable native defect across all Fermi levels under Ga-rich conditions, and V_{Ga} is the lowest-energy acceptor for *n*-type conditions.

The results presented in Fig. 3b are qualitatively quite similar to previous LDA and PBE calculations which included neither band-edge shifts nor finite-size corrections (but which extended the Fermi level beyond the LDA-calculated CBM in similar plots). As noted in ref. 61, the apparent accuracy of the old LDA or PBE calculations is due to a fortuitous cancellation of errors: the shift of the band edges (when a more accurate functional is applied) causes a lowering of formation energies for defects that are positively charged at the VBM. Counteracting this shift is the application of finite-size corrections, which cause charged-defect energies to increase.

A comparison of the thermodynamic transition levels calculated within shifted GGA and HSE for each individual defect is shown in Fig. 4. Overall, we find a mean average error of 0.24 eV for defect transition levels, once band-edge shifts are taken into account, again indicating that when band edges are appropriately aligned, GGA results can produce qualitatively accurate results. However, as discussed in Native defects in GaN, a larger discrepancy is found for *optical* transition levels even when calculated thermodynamic transition levels are in close agreement, specifically in the case of V_{Ga} and V_N. We connect this disparity to the failure of GGA to fully describe charge localization and concurrent relaxations around defects. The disagreement in calculated optical levels suggests that, at least in certain cases, fully consistent hybrid functional calculations are necessary to obtain an accurate physical description of defects.

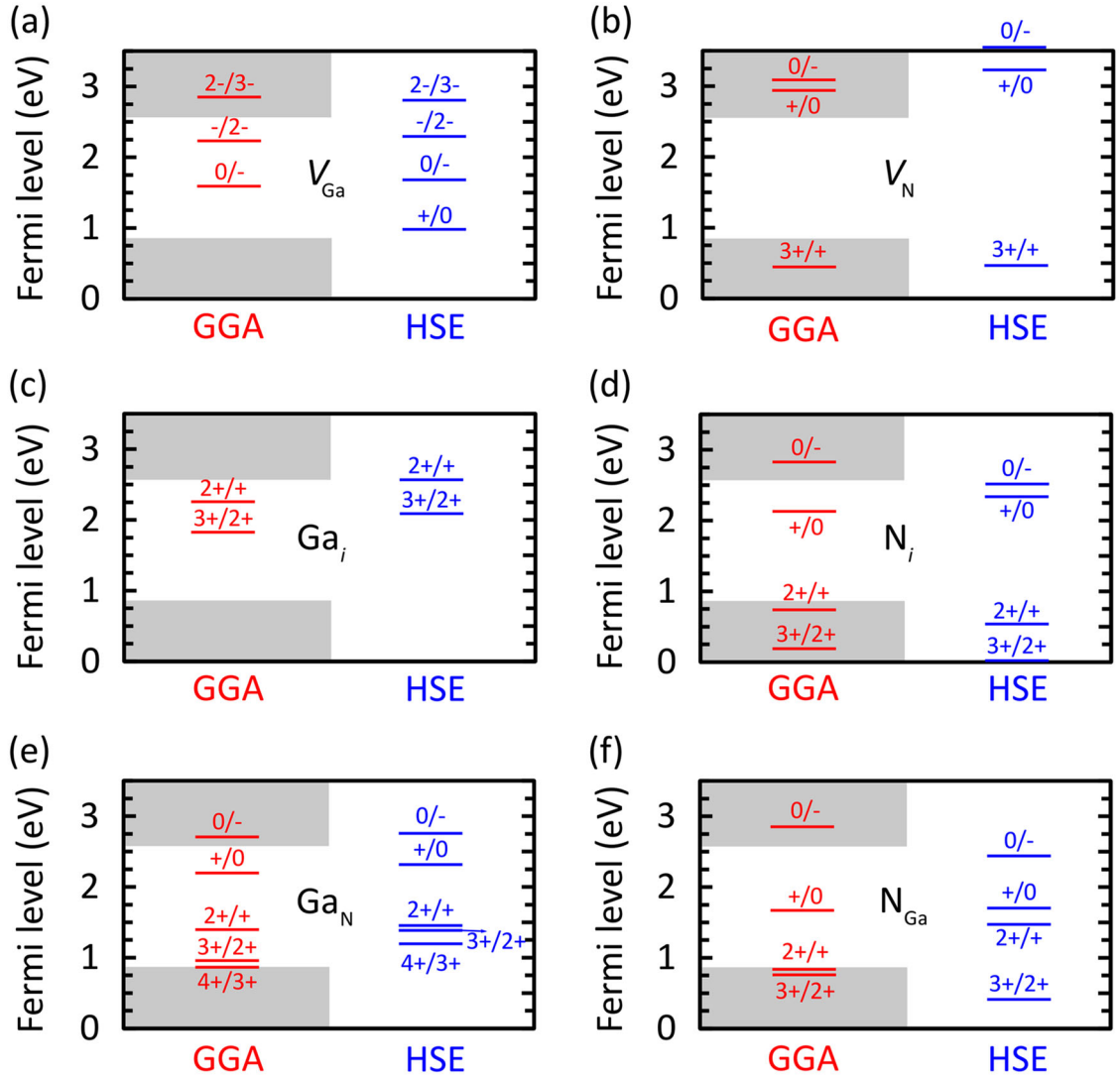

Fig. 4 Comparison of thermodynamic transition levels for **a** the gallium vacancy (V_{Ga}), **b** nitrogen vacancy (V_N), **c** gallium self-interstitial (Ga_i), **d** nitrogen self-interstitial (N_i), **e** gallium antisite (Ga_N), and **f** nitrogen antisite (N_{Ga}) in GaN calculated with GGA (PBE) (left part of each panel, in *red*) and HSE (right part of each panel, in *blue*). Areas in *grey* in the GGA plots are Fermi levels that reside outside the GGA band extrema

Native defects in GaN

Gallium vacancies. Early calculations based on the LDA indicated that gallium vacancies would be the most important native compensating acceptors in GaN, and that they would act as a source of yellow luminescence.[13, 64] While both of these statements remain true, the more recent HSE results have shed new light on the issues and forced a reassessment of the quantitative details.

Thermodynamic transition levels. The early calculations reported a (2−/3−) transition level at 1.1 eV above the VBM.[64] Using sx-LDA, and the finite-size corrections as described in ref. 25, ref. 62 reported a (2−/3−) transition level 2.09 eV above the VBM. An upward shift in V_{Ga} transition levels was also observed in HSE calculations,[53] and linked to the trapping of holes in polaronic states localized on the N atoms nearest to the vacancy site. Such a localization is not captured at all in LDA or GGA. A correct description of the physics causes charge-state transition levels to shift upward with respect to the VBM.

We note that the upward shift in the defect level, compared to the old LDA results, is only partly due to the functional; a sizeable shift also occurs due to the application of the finite-size supercell correction, which increases the energies of charged states and is proportional to the square of the charge state. In our calculations, the correction for the 2− charge state amounts to 1.10 eV, while for the 3− charge state it is 2.22 eV; the net effect is to shift the (2−/3−) transition level towards the CBM by 1.12 eV.

In our own hybrid functional calculations[53] we found the (0/−) level at 1.68 eV, the (−/2−) level at 2.33 eV, and the (2−/3−) at 2.80 eV. Comparing our "shifted" GGA values with full HSE values, shown in Fig. 4a, indicates that the shifted GGA values are somewhat lower (by 0.2 eV) than the HSE values.

Overall, defect levels for V_{Ga} obtained with GGA combined with band-edge shifts seem to provide a reasonable approximation for transition energies, although the inability of GGA to capture hole localization leads to some quantitative differences. A major discrepancy occurs, however, for the (+/0) transition level of V_{Ga}. Our HSE calculations show the + charge state to be stable for low Fermi levels, and produce a (+/0) level at 0.97 eV. The stability of the + charge state is related to the ability of V_{Ga} to strongly trap a fourth hole,[53] as described within HSE. Within GGA, we find that a fourth hole cannot be trapped at V_{Ga}. Although such a state is reported in ref. 54, we find that when the defect is placed in a +

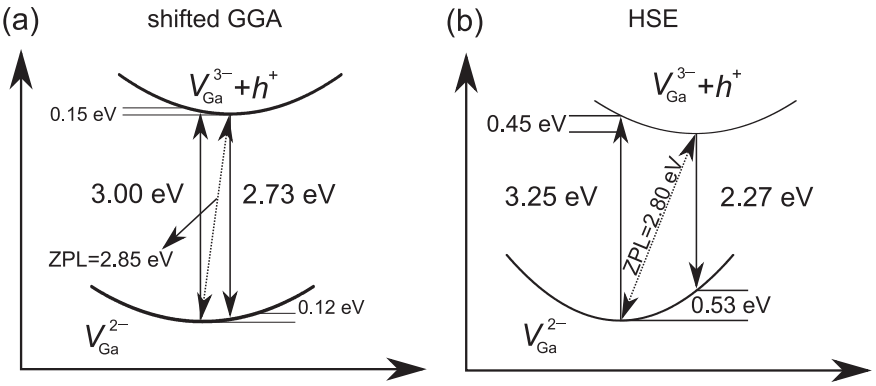

Fig. 5 Comparison of the **a** GGA- and **b** HSE-calculated CC diagrams for optical transitions involving capture of a hole by V_{Ga}^{3-}

charge state, this hole resides in a delocalized, valence-band-related state. For this reason, the (+/0) transition level is not shown in Fig. 4a.

Optical transition levels. Although thermodynamic transition levels are reasonably well described by the "shifted GGA" calculations, examination of optical transitions reveals significant discrepancies. As an illustration, we examine transitions involving hole capture into the (2−/3−) level for both shifted GGA and HSE, as shown in Fig. 5.

The HSE-calculated atomic configurations of the 3− and 2− charge states of V_{Ga} are quite different. For V_{Ga}^{2-}, there is a characteristic, outwards relaxation of a single N neighbor from V_{Ga}^{2-} by 12% of the GaN bulk bond length, concurrent with the localization of a hole onto this N atom. There is no hole present for V_{Ga}^{3-} (all defect states are filled), and all nearest neighbors move outwards by 7–9% of the GaN bond length. This leads to large relaxation energies (also known as the Franck-Condon shift[29]) of approximately 0.5 eV, and this in turn leads to the peak absorption (3.25 eV) and emission (2.27 eV) energies being significantly shifted from the zero-phonon line (ZPL; 2.80 eV), as shown in Fig. 5b. The CC diagram calculated with HSE thus explains how V_{Ga} can give rise to yellow luminescence (see Table 1) despite the (2−/3−) transition level being so near to the CBM.[53] Rather than an *electron* being captured at a V_{Ga}^{2-} center, as had been previously assumed,[13, 64] the transition involves a *hole* being captured at V_{Ga}^{3-}. The latter is, in fact, expected to be a stronger transition, based on the Coulomb interaction between the band-edge carrier and the defect center.

In contrast to HSE, within GGA there is no anisotropic distortion for V_{Ga}^{2-}. Instead, all N atoms move outwards by between 7 and 8% of the Ga–N bond length. For V_{Ga}^{3-}, the nearest-neighbor N atoms move away from the vacant site by 6 to 7%. The similarity in these atomic configurations causes the relaxation energy to be on the order of only 0.1 eV within GGA. Thus, although the ZPL for the shifted GGA results shown in Fig. 5a is in close agreement with the HSE value (after inclusion of the band-edge shifts), the predicted peak energies for optical transitions (3.00 eV for absorption and 2.73 eV for emission) are much closer to the ZPL than is found for HSE.

The results for V_{Ga} present a potential pitfall in using shifted GGA results to predict the properties of defects in semiconductors. Although the thermodynamic transition levels might be described with acceptable accuracy once band-edge shifts are taken into account, this does not guarantee that all properties of the defect will be similarly well described. In particular, cases involving carrier localization, which in turn affects the magnitude of atomic relaxations, are likely to be poorly described by semilocal DFT. This affects the relative position of the minima of the curves for different charge states in the CC diagram, as has been shown here for V_{Ga}, and leads to incorrect predictions of the optical transition energies.

Table 1. Gallium-vacancy-related levels that can give rise to yellow luminescence in GaN

Defect	level	(q/q') (eV)	ZPL (eV)	PL peak (eV)
V_{Ga}	(2−/3−)	2.80	2.80	2.27
V_{Ga}–3H	(+/0)	0.73	2.77	2.05
V_{Ga}–O_N–2H	(+/0)	0.92	2.58	1.90

For each species, the charge-state transition level is identified and its energy (q/q') (referenced to the VBM) is listed. The ZPL and predicted photoluminescence (PL) peak energy of the associated optical transition are also listed. The V_{Ga} transition involves capturing holes from the VBM; the transitions for complexes involve capturing electrons from the CBM

Formation energies. We now comment on the formation energy of V_{Ga}. The early LDA calculations reported a formation energy of about 1.3 eV under Ga-rich conditions when the Fermi level is at the CBM (*n*-type conditions).[64] This relatively low value seemed to indicate that Ga vacancies would be relatively abundant, a prediction that seemed to be confirmed by positron annihilation experiments.[65, 66] The HSE calculations (as well as "shifted GGA") calculations, however, produce a much higher formation energy, about 4.5 eV in HSE. This high value indicates that Ga vacancies are highly unlikely to occur in as-grown GaN, even if the chemical potentials would shift away from the extreme Ga-rich limit. (We note here that observations of V_{Ga}, such as in ref. 67, occurred in irradiated GaN samples.) Does that mean that Ga vacancies are irrelevant? Not at all. As we will discuss in the next section, complexes can form between Ga vacancies and unintentional donor impurities such as hydrogen or oxygen, significantly lowering the formation energy and making incorporation of such vacancy-related complexes more likely. Indeed, more recent positron annihilation experiments[68, 69] have acknowledged that while "bare" Ga vacancies are observed in intentionally damaged material, the Ga vacancies observed in as-grown material are very likely complexed with impurities such as hydrogen.

Donor-gallium-vacancy complexes. It is natural to expect that donor impurities will tend to form complexes with gallium vacancies, which act as deep acceptors. Donor-gallium-vacancy complexes were discussed as compensating defects as well as sources of broad-band luminescence.[13, 64, 70] Oxygen and hydrogen are known to be common unintentional impurities in nitride growth. Oxygen resides on the nitrogen site (O_N), where it acts as a singly charged shallow donor; in a complex with a

gallium vacancy, the oxygen replaces a nitrogen atom adjacent to the vacancy site. Interstitial hydrogen (H_i) is in principle amphoteric, but it acts as a donor when forming a complex with negatively charged V_{Ga}; hydrogen can bond to one or more N neighbors of the vacancy.

Such complexes (as well as complexes involving both oxygen and hydrogen) have lower formation energies than the bare vacancy and thus have a higher likelihood of incorporating in as-grown GaN.[53] They have been observed experimentally using electron paramagnetic resonance[71] as well as positron annihilation.[68, 69, 72] Vacancy-donor complexes have also been identified as a source of nonradiative recombination in GaN and In GaN alloys.[7, 8]

Recent hybrid functional calculations[53] have confirmed that both oxygen- and hydrogen-vacancy complexes are quite stable. Their stability is illustrated by the large values of "removal energies" (over 3 eV); these removal energies are calculated by taking the difference between the formation energy of the complex and the sum of the formation energies of the donor impurity and of the entity that is left when the donor is taken away.[53] Similar to the case of the isolated vacancy, such vacancies can trap holes and give rise to optical transition energies that are strongly shifted from the ZPL. Also similar to V_{Ga}, such complexes can bind an additional hole even after forming a complex with three donor impurities, i.e., a situation in which the vacancy has in principle been completely "neutralized". Thus, even the neutral V_{Ga}-3H and V_{Ga}-O_N-2H complexes, which do not act as compensating centers any more, exhibit a (+/0) transition level in the band gap, which can still give rise to vacancy-related yellow luminescence[53] (see Table 1). We should note that V_{Ga} and related complexes are not the only sources of yellow luminescence in GaN; the carbon acceptor (C_N) in GaN also has been implicated in causing such transitions.[73]

Nitrogen vacancies

Prior to the 1990s, unintentional *n*-type conductivity in GaN was attributed to the presence of V_N.[74] Early LDA calculations[10, 13] seemed to confirm that V_N acted as a shallow donor, but more importantly, they found that this defect had a very high formation energy under *n*-type conditions. This has turned out to be a robust result, forcing the conclusion that V_N is unlikely to incorporate in significant concentrations in *n*-type GaN and thus cannot be responsible for *n*-type conductivity. Unintentional *n*-type conductivity, instead, had to be attributed to unintentional incorporation of impurities,[10] which led to a concerted effort to control incorporation of such impurities (in particular oxygen and silicon).

Thermodynamic transition levels. Later computational work[75] continued to highlight V_N as the most important native defect in GaN, but also identified charge states up to 3− for this defect. In contrast, hybrid functional calculations[76] (see also Fig. 3b) find that the highest stable charge state is the neutral charge state. Calculations such as ref. 75 find the higher charge states to be stable because they are based on LDA results combined with a rigid, upwards "scissors shift" of the CBM in order to correct the band gap. As a result of this shift, spurious charge states appear to become stable. A similar effect is seen in Fig. 3a: use of GGA results combined with an extension of the band gap lead to the appearance of the V_N^- being stable at high Fermi levels, in contrast to HSE calculations which show the neutral charge state to be the highest stable charge state.

Utilizing HSE calculations with finite-size corrections, Yan *et al.*[76] found that V_N gives rise to two charge-state transition levels within the GaN band gap: a (3+/+) level at 0.47 eV above the VBM, and a (+/0) level 0.24 eV below the CBM (see Fig. 6). The presence of the (3+/+) transition level indicates that V_N acts as a "negative-*U*" center in GaN, meaning that a given charge state (in this case, 2+)

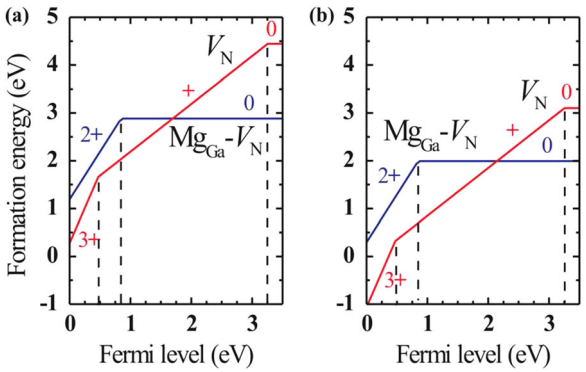

Fig. 6 Formation energy plots of V_N and the Mg_{Ga}-V_N complex for **a** N-poor and **b** N-rich conditions. Reprinted from Ref. 76 with the permission of AIP Publishing

is not stable over any region of the semiconductor band gap. Results similar to the HSE calculations were found in other studies employing hybrid functionals.[77, 78] However, V_N^0 was not found to be stable in ref. 78, and the (0/−) transition level was found to occur 4 meV below the CBM in ref. 77.

The HSE-calculated (3+/+) level compares well with the shifted GGA value shown in Fig. 4b, which occurs 0.45 eV above the VBM. The agreement for the (+/0) level is not as good; the shifted GGA value occurs 0.53 eV below the CBM. The (0/−) transition level, calculated to occur 0.04 eV above the CBM in HSE, occurs 0.38 eV below the CBM within the shifted GGA results.

A hybrid functional study using an embedded cluster approach found V_N to be a shallow donor in GaN.[79] However, it is unclear if the stability of V_N^0 was explored in this work, making a full comparison with the results of ref. 76 difficult. We note that the same study[79] found the (0/−) level of Mg_{Ga} to be located at 1.40 eV above the VBM. Magnesium is well established to be an acceptor that dopes GaN *p* type, with an ionization energy of ~200 meV.[80] The results of ref. 79 thus overestimate the position of the transition level by more than 1 eV, casting doubt on the reliability of any of the transition levels calculated within that study.

Optical transition levels. The HSE results[76] also indicate that transitions of electrons into the (3+/2+) level of V_N give rise to broad, yellow luminescence peaking near 2.18 eV, with a large relaxation energy of 0.81 eV and an ZPL at 2.99 eV.[76] A similar optical transition was calculated in ref. 77. This transition would explain the occurrence of yellow luminescence in *p*-type GaN,[81, 82] in which nitrogen vacancies are expected to occur as compensating centers due to their low formation energies. Other sources of yellow luminescence, such as Ga vacancies (or their complexes, as discussed above) or carbon[32, 73] are less likely to be present in *p*-type GaN.

As was observed for V_{Ga}, we find that optical transitions calculated for V_N within shifted GGA also deviate from HSE values, despite the fact that the (3+/+) agrees to within 0.02 eV between shifted-GGA and HSE. With shifted GGA, we obtain a ZPL of 3.21 eV and a relaxation energy of 0.65 eV. This gives a predicted peak luminescence of 2.56 eV, a difference of 0.38 eV from the HSE value. We again attribute this discrepancy to the distinct charge-state relaxation calculated within each functional. Whereas HSE predicts outwards relaxations of 22% (for V_N^{3+}) and 11% (for V_N^{2+}) for nearest-neighbor Ga atoms, within PBE these same relaxations are only 17% (V_N^{3+}) and 6% (V_N^{2+}).

Nitrogen-vacancy complexes. Although isolated V_N has a high formation energy in *n*-type conditions, it can interact with hydrogen impurities to form substitutional H_N,[70] which is a

double donor. However, since H_N has a high formation energy in *n*-type material it is unlikely to form in significant concentrations. Freysoldt *et al.*[61] found agreement within 0.1 eV for the formation energy of H_N^{2+} when comparing hybrid functional calculations with GGA and LDA calculations, once VBM shifts and chemical potentials were properly taken into account.

While the formation energy of V_N is high in *n*-type GaN, it becomes much lower when the Fermi level is closer to the VBM (see Fig. 3). This indicates that nitrogen vacancies act as compensating centers in *p*-type GaN. In addition, since they occur in a + or 3+ charge state, it is expected that they would be attracted to negatively charged Mg_{Ga} centers and form V_N-Mg_{Ga} complexes.[83]

The hybrid functional calculations of Yan *et al.*[76] (Fig. 6) indeed showed that V_N forms stable complexes with Mg_{Ga}, and that such complexes give rise to deep donor transition levels near the VBM. These results indicated that positively charged Mg_{Ga}-V_N complexes might be an important source of compensation in Mg-doped GaN, and that such complexes could give rise to characteristic 1.8 eV red luminescence.[76] Similar optical activity arising from Mg_{Ga}-V_N was reported in ref. 77.

Gallium interstitials

LDA calculations established that Ga_i incorporates in the octahedral site (as in Fig. 1c) and acts as a donor.[21] These calculations identified a single (3+/+) transition level for Ga_i, at 2.5 eV above the VBM. In the 3 + charge state of Ga_i all defect levels are empty; occupying the defect states of Ga_i (with two electrons in the case of Ga_i^+) leads to the stabilization of lower charge states. With shifted GGA we find two transition levels that occur somewhat lower in the band gap, a (3+/2+) level at 1.83 eV and a (2+/+) level at 2.26 eV above the VBM.

The appearance of the (3+/2+) and (2+/+) levels, which were absent in the LDA calculations[21] is due to the fact that the energy of the 2+ state was too high in the LDA calculations. This was due to two factors: the neglect of spin polarization in the LDA calculations, and the lack of charge-state corrections which were not available at the time of the calculations reported in ref. 21. The charge-state correction scales as q^2 and is hence particularly large for the 3+ state, raising its energy with respect to the 2+ state. This results in Ga_i no longer being a negative-*U* center (since the 2+ charge state is now stable over some range of Fermi levels), and leads to the appearance of the (3+/2+) and (2+/+) transition levels in the gap. These results are confirmed by our hybrid functional calculations: we find the (3+/2+) level is 2.09 eV above the VBM and the (2+/+) level to be 2.57 eV above the VBM.

Due to its high formation energy, Ga_i is not expected to influence electrical conductivity in GaN. Although the formation energy becomes lower under *p*-type conditions (Fig. 3), compensation of *p*-type conductivity is more likely to be caused by the lower-energy V_N donors. Gallium interstitials have been observed experimentally in GaN, but only when created by irradiation at 4.2 K and if the sample is kept at low temperatures.[84] The interstitials become mobile below room temperature. The low diffusion barrier and high formation energy of Ga_i preclude this defect from affecting the properties of as-grown GaN.

Nitrogen interstitials

LDA calculations[85] found that N_i incorporates in the split-interstitial position similar to the one depicted in Fig. 1d, in which two N atoms share a substitutional lattice site and form close, 1.1–1.4 Å bonds; the precise details of the atomic geometry depend on the charge state. N_i gives rise to four transition levels within the band gap of GaN. It was found to be stable in positively charged states when the Fermi level is in the lower part of the band gap, becoming negatively charged at higher Fermi levels.

Our HSE calculations confirm that N_i incorporates as a split interstitial and gives rise to four transition levels. The HSE (shifted GGA) transition levels are at 0.02 (0.19) eV for the (3+/2+) level, 0.54 (0.74) eV for the (2+/+) level, 2.34 (2.13) eV for the (+/0) level, and 2.52 (2.83) eV for the (0/−) level. The 0.2–0.3 eV discrepancy is in line with the expected difference between HSE and shifted GGA transition levels (which has an overall average of 0.24 eV). Our results are consistent with the electron paramagnetic resonance experiments that identified N_i (created by particle irradiation) as a split interstitial with a (0/−) level ~1 eV from the CBM,[86] as well as with the HSE results reported in that reference.

Gallium antisites

Occupation of the N site by a Ga atom leads to the Ga antisite (Ga_N), as depicted in Fig. 1e. This center was found by LDA calculations to give rise to five transition levels and to have a large formation energy.[21] Similar results are found here in the HSE and shifted GGA calculations, as shown in Figs. 3 and 4e. The HSE-calculated (2+/+), (+/0), and (0/−) levels of Ga_N all lie within 0.15 eV of the shifted GGA results. For the (4+/3+) level (1.2 eV above the VBM in HSE vs. 0.87 eV in shifted GGA) and the (3+/2+) level (1.39 eV above the VBM in HSE vs. 0.96 eV in shifted GGA) the discrepancies are larger. Since these highly charged 4+ and 3+ states of Ga_N feature holes localized onto N atoms, we attribute this discrepancy to the inability of GGA to fully capture hole localization, as was the case for the positively charge states of V_{Ga} and related complexes. Overall, Ga_N exhibits high formation energies in GaN and is not expected to play a role.

Nitrogen antisites

As shown in Fig. 1f, occupation of the Ga site by N leads to significant distortions of the GaN lattice, involving the formation of close N-N bonds between N_{Ga} and neighboring N atoms. The need for strong distortions gives rise to its high formation energy, and previous studies have already dismissed this defect as having negligible influence in GaN.[21]

The HSE results for N_{Ga} are similar to the shifted GGA results. As shown in Fig. 3f, both lead to four transition levels occurring in the band gap. However, the disagreement in transition levels between HSE and shifted GGA is largest for this center: 0.43 eV for the (3+/2+) transition, 0.71 eV for the (2+/+) level, 0.03 eV for the (+/0) level, and 0.41 eV for the (0/−) level. We again attribute this discrepancy to the fact that GGA does not appropriately capture the behavior of the localized N states that compose the N_{Ga} defect levels. As with Ga_N, the high formation energy of N_{Ga} over all Fermi levels precludes this defect from affecting the properties of GaN.

CONCLUSIONS

We have reviewed first-principles calculations of native point defects in GaN. We focused on two important advances made over the last decade, namely the incorporation of charge-state correction schemes, and the use of functionals that go beyond local or semilocal DFT functionals. Our benchmark has been based on hybrid functional calculations, which have been established not only to address the band-gap underestimation inherent in LDA and GGA, but also to provide a reliable description of carrier localization; the latter phenomenon can affect defect energies, particularly in cases where holes localize on dangling bonds.

Correctly incorporating charge-state corrections can be done with little computational effort; but going beyond LDA or GGA involves significant computational expense, and hence it is important to examine to what extent LDA or GGA calculations can be relied upon to perform large-scale or high-throughput calculations. In addition, such an examination sheds light on the reliability of some of the older studies in the literature.

Semilocal DFT functionals underestimate the band gap of GaN, and this error affects the position of defect levels within the band gap and the values of formation energies. A major part of this error can be corrected by correcting for the band-edge positions: i.e., using formation energies and defect levels as calculated with GGA, but interpreting them within a band gap where the valence-band edge has been shifted down, and the conduction-band edge has been shifted up. We have shown that this type of correction scheme (also used in Ref. 54) produces results for thermodynamic transition levels that agree with full hybrid functional calculations to within 0.24 eV on average.

However, this overall agreement masks specific cases where much larger discrepancies occur; these are associated with situations in which carrier localization occurs. The inadequate description of hole localization within semilocal functionals such as GGA can lead to differences in atomic relaxations, which gives rise to significant errors when optical transitions are examined. We highlighted these deficiencies in the case of V_{Ga} and V_N, the defects with lowest formation energy that are expected to play the most important role in GaN.

The bottom line is that lower-cost functionals such as GGA, combined with band-edge correction schemes, can produce results that are qualitatively (and sometimes even quantitatively) correct, but that important physics may be missed in cases that turn out to be most important, from the point of view of impact on experimental materials properties.

ACKNOWLEDGEMENTS

J. L. was supported by the Center for Low Energy Systems Technology (LEAST), one of the six SRC STARnet Centers, sponsored by MARCO and DARPA. C. V. d. W. was supported by the US Department of Energy (DOE), Office of Science, Basic Energy Sciences (BES) under Award No. DE-SC0010689. Computational resources were provided by the Center for Scientific Computing at the California Nanosystems Institute and Materials Research Laboratory (an NSF Materials Research Science and Engineering Center, DMR-1121053) (NSF CNS-0960316), by the Extreme Science and Engineering Discovery Environment (XSEDE), supported by NSF (ACI-1053575), and by the National Energy Research Scientific Computing Center, a DOE Office of Science User Facility supported by the Office of Science of the U.S. Department of Energy under Contract No. DE-AC02-05CH11231.

COMPETING INTERESTS

The authors declare that they have no competing interests.

REFERENCES

1. Pimputkar, S., Speck, J. S., DenBaars, S. P. & Nakamura, S. Prospects for LED lighting. *Nat. Photonics* **3**, 180–182 (2009).
2. Jani, O., Ferguson, I., Honsberg, C. & Kurtz, S. Design and characterization of GaN/InGaN solar cells. *Appl. Phys. Lett.* **91**, 132117 (2007).
3. Mishra, U. K., Shen, L., Kazior, T. E. & Wu, Y.-F. GaN-based RF power devices and amplifiers. *P. IEEE* **96**, 287–305 (2008).
4. Yoshida, M. *et al.* Photoluminescence spectroscopic and computational investigation of the origin of the visible light response of Ga(1-x)Zn(x)N(1-x)O(x) photocatalyst for overall water splitting. *J. Phys. Chem. C* **114**, 15510–15515 (2010).
5. Sztein, A., Bowers, J. E., DenBaars, S. P. & Nakamura, S. Polarization field engineering of GaN/AlN/AlGaN superlattices for enhanced thermoelectric properties. *Appl. Phys. Lett.* **104**, 042106 (2014).
6. Varley, J. B., Janotti, A. & Van de Walle, C. G. Defects in AlN as candidates for solid-state qubits. *Phys. Rev. B* **93**, 161201R (2016).
7. Dreyer, C. E., Alkauskas, A., Lyons, J. L., Speck, J. & Van de Walle, C. G. Gallium vacancy complexes as a cause of Shockley-Read-Hall recombination in III-nitride light emitters. *Appl. Phys. Lett.* **108**, 141101 (2016).
8. Alkauskas, A., Dreyer, C. E., Lyons, J. L. & Van de Walle, C. G. Role of excited states in Shockley-Read-Hall recombination in wide-band-gap semiconductors. *Phys. Rev. B* **93**, 201304R (2016).
9. Tansley, T. L. & Egan, R. J. Point-defect energies in the nitrides of aluminum, gallium, and indium. *Phys. Rev. B* **45**, 10942–10950 (1992).
10. Neugebauer, J. & Van de Walle, C. G. Atomic geometry and electronic structure of native defects in GaN. *Phys. Rev. B* **50**, 8067R–8070R (1994).
11. Bogusławski, P., Briggs, E. L. & Bernholc, J. Native defects in gallium nitride. *Phys. Rev. B* **51**, 17255R–17259R (1995).
12. Estreicher, S. K. *et al.* (eds.) *GaN and Related Materials* (Gordon and Breach, 1997).
13. Mattila, T. & Nieminen, R. M. Point-defect complexes and broadband luminescence in GaN and AlN. *Phys. Rev. B* **55**, 9571–9576 (1997).
14. Gorczyca, I., Svane, A. & Christensen, N. E. Theory of point defects in GaN, AlN, and BN: relaxation and pressure effects. *Phys. Rev. B* **60**, 8147–8157 (1999).
15. Hohenberg, P. & Kohn, W. Inhomogeneous electron gas. *Phys. Rev* **136**, B864–B871 (1964).
16. Kohn, W. & Sham, L. J. Self-consistent equations including exchange and correlation effects. *Phys. Rev* **140**, A1133–A1138 (1965).
17. Ceperley, D. M. & Alder, B. J. Ground-state of the electron-gas by a stochastic method. *Phys. Rev. Lett.* **45**, 566–569 (1980).
18. Perdew, J. P. & Zunger, A. Self-interaction correction to density-functional approximations for many-electron systems. *Phys. Rev. B* **23**, 5048–5079 (1981).
19. Perdew, J. P., Burke, K. & Ernzerhof, M. Generalized gradient approximation made simple. *Phys. Rev. Lett.* **77**, 3865–3868 (1996).
20. Becke, A. A new mixing of Hartree-Fock and local density-functional theories. *J. Chem. Phys.* **98**, 1372–1377 (1993).
21. Van de Walle, C. G. & Neugebauer, J. First-principles calculations for defects and impurities: applications to III-nitrides. *J. Appl. Phys.* **95**, 3851–3879 (2004).
22. Freysoldt, C. *et al.* First-principles calculations for point defects in solids. *Rev. Mod. Phys.* **86**, 253–305 (2014).
23. Komsa, H.-P., Rantala, T. T. & Pasquarello, A. Finite-size supercell correction schemes for charged defect calculations. *Phys. Rev. B* **86**, 045112 (2012).
24. Lany, S. & Zunger, A. Assessment of correction methods for the band-gap problem and for finite-size effects in supercell defect calculations: case studies for ZnO and GaAs. *Phys. Rev. B* **78**, 235104 (2008).
25. Freysoldt, C., Neugebauer, J. & Van de Walle, C. G. Fully *ab initio* finite-size corrections for charged-defect supercell calculations. *Phys. Rev. Lett.* **102**, 016402 (2009).
26. Freysoldt, C., Neugebauer, J. & Van de Walle, C. G. Electrostatic interactions between charged defects in supercells. *Phys. Status Solidi B* **248**, 1067–1076 (2011).
27. Blöchl, P. E. Projector augmented-wave method. *Phys. Rev. B* **50**, 17953 (1994).
28. Kresse, G. & Furthmüller, J. Efficient iterative schemes for *ab initio* total-energy calculations using a plane-wave basis set. *Phys. Rev. B* **54**, 11169 (1996).
29. Alkauskas, A., McCluskey, M. D. & Van de Walle, C. G. Tutorial: defects in semiconductors-combining experiment and theory. *J. Appl. Phys.* **119**, 181101 (2016).
30. Heyd, J., Scuseria, G. E. & Ernzerhof, M. Hybrid functionals based on a screened coulomb potential. *J. Chem. Phys.* **118**, 8207–8215 (2003).
31. Heyd, J., Scuseria, G. E. & Ernzerhof, M. Erratum: hybrid functionals based on a screened Coulomb potential. *J. Chem. Phys.* **124**, 219906 (2006).
32. Lyons, J. L., Janotti, A. & Van de Walle, C. G. Effects of carbon on the electrical and optical properties of InN, GaN, and AlN. *Phys. Rev. B* **89**, 035204 (2014).
33. Rinke, P., Qteish, A., Neugebauer, J., Freysoldt, C. & Scheffler, M. Combining *GW* calculations with exact-exchange density-functional theory: an analysis of valence-band photoemission for compound semiconductors. *New J. Phys.* **7**, 126 (2005).
34. Punya, A. & Lambrecht, W. R. L. Valence band effective-mass Hamiltonians for the group-III nitrides from quasiparticle self-consistent *GW* band structures. *Phys. Rev. B* **85**, 195147 (2012).
35. Rinke, P., Janotti, A., Scheffler, M. & Van de Walle, C. G. Defect formation energies without the band-gap problem: Combining density-functional theory and the *GW* approach for the silicon self-interstitial. *Phys. Rev. Lett.* **102**, 026402 (2009).
36. Rinke, P. *et al.* First-principles optical spectra for *F* Centers in MgO. *Phys. Rev. Lett.* **108**, 126404 (2012).
37. Santana, J. A., Krogel, J. T., Kim, J., Kent, P. R. C. & Reboredo, F. A. Structural stability and defect energetics of ZnO from diffusion quantum Monte Carlo. *J. Chem. Phys.* **142**, 164705 (2015).
38. Ertekin, E., Wagner, L. K. & Grossman, J. C. Point-defect optical transitions and thermal ionization energies from quantum Monte Carlo methods: application to the F-center defect in MgO. *Phys. Rev. B* **87**, 155210 (2013).
39. Parker, W. D., Wilkins, J. W. & Hennig, R. G. Accuracy of quantum Monte Carlo methods for point defects in solids. *Phys. Status Solidi B* **248**, 267–274 (2011).
40. Janotti, A., Segev, D. & Van de Walle, C. G. Effects of cation *d* states on the structural and electronic properties of III-nitride and II-oxide wide-band-gap semiconductors. *Phys. Rev. B* **74**, 045202 (2006).
41. Lany, S. & Zunger, A. Polaronic hole localization and multiple hole binding of acceptors in oxide wide-gap semiconductors. *Phys. Rev. B* **80**, 085202–085205 (2009).
42. Chakrabarty, A. & Patterson, C. H. Transition levels of defects in zno: total energy and janakâs theorem methods. *J. Chem. Phys.* **137**, 054709 (2012).
43. Li, Y., Sanna, S. & Schmidt, W. G. Modeling intrinsic defects in $LiNbO_3$ within the slater-janak transition state model. *J. Chem. Phys.* **140**, 234113 (2014).

44. Van de Walle, C. G. & Segev, D. Microscopic origins of surface states on nitride surfaces. *J. Appl. Phys.* **101**, 081704 (2007).
45. Tran, F. & Blaha, P. Accurate band gaps of semiconductors and insulators with a semilocal exchange-correlation potential. *Phys. Rev. Lett.* **102**, 226401 (2009).
46. Landmann, M. *et al.* Transition energies and direct-indirect band gap crossing in zinc-blende $Al_xGa_{1-x}N$. *Phys. Rev. B* **87**, 195210 (2013).
47. Batista, E. R. *et al.* Comparison of screened hybrid density functional theory to diffusion Monte Carlo in calculations of total energies of silicon phases and defects. *Phys. Rev. B* **74**, 121102R (2006).
48. Deák, P., Aradi, B., Frauenheim, T., Janzén, E. & Gali, A. Accurate defect levels obtained from the HSE06 range-separated hybrid functional. *Phys. Rev. B* **81**, 153203 (2010).
49. Ágoston, P., Albe, K., Nieminen, R. M. & Puska, M. J. Intrinsic *n*-type behavior in transparent conducting oxides: a comparative hybrid-functional study of In_2O_3, SnO_2, and ZnO. *Phys. Rev. Lett.* **103**, 245501 (2009).
50. Alkauskas, A. & Pasquarello, A. Band-edge problem in the theoretical determination of defect energy levels: the O vacancy in ZnO as a benchmark case. *Phys. Rev. B* **84**, 125206R (2011).
51. Komsa, H.-P. & Pasquarello, A. Assessing the accuracy of hybrid functionals in the determination of defect levels: application to the As antisite in GaAs. *Phys. Rev. B* **84**, 075207 (2011).
52. Hoang, K. Hybrid density functional study of optically active Er^{3+} centers in GaN. *Phys. Status Solidi Rapid Res. Lett.* **9**, 722–725 (2015).
53. Lyons, J. L., Alkauskas, A., Janotti, A. & Van de Walle, C. G. First-principles theory of acceptors in nitride semiconductors. *Phys. Status Solidi B* **252**, 900–908 (2015).
54. Miceli, G. & Pasquarello, A. Energetics of native point defects in GaN. *Microelectron. Eng.* **147**, 51–54 (2015).
55. Demchenko, D. O. & Reshchikov, M. A. Blue luminescence and Zn acceptor in GaN. *Phys. Rev. B* **88**, 115204 (2013).
56. Collazo, R. *et al.* On the origin of the 265nm absorption band in AlN bulk crystals. *Appl. Phys. Lett.* **100**, 191914 (2012).
57. Vurgaftman, I. & Meyer, J. R. Band parameters for nitrogen-containing semiconductors. *J. Appl. Phys.* **94**, 3675–3696 (2003).
58. Hautier, G., Miglio, A., Ceder, G., Rignanese, G.-M. & Gonze, X. Identification and design principles of low hole effective mass *p*-type transparent conducting oxides. *Nat. Commun.* **14**, 2292 (2013).
59. Alkauskas, A., Broqvist, P. & Pasquarello, A. Defect energy levels in density functional calculations: alignment and band gap problem. *Phys. Rev. Lett.* **101**, 046405 (2008).
60. Lyons, J. L., Janotti, A. & Van de Walle, C. G. Role of Si and Ge as impurities in ZnO. *Phys. Rev. B* **80**, 205113 (2009).
61. Freysoldt, C. *et al.* Electron and chemical reservoir corrections for point-defect formation energies. *Phys. Rev. B* **93**, 165206 (2016).
62. Gillen, R. & Robertson, J. A hybrid density functional view of native vacancies in gallium nitride. *J. Phys.-Condens. Mat* **25**, 405501 (2013).
63. Bylander, D. M. & Kleinman, L. Good semiconductor band gaps with a modified local-density approximation. *Phys. Rev. B* **41**, 7868–7871 (1990).
64. Van de Walle, C. G. & Neugebauer, J. Gallium vacancies and the yellow luminescence in GaN. *Appl. Phys. Lett.* **69**, 503–505 (1996).
65. Saarinen, K. *et al.* Observation of native Ga vacancies in GaN by positron annihilation. *Phys. Rev. Lett.* **79**, 3030–3033 (1997).
66. Oila, J. *et al.* Ga vacancies as dominant intrinsic acceptors in GaN grown by hydride vapor phase epitaxy. *Appl. Phys. Lett.* **82**, 3433–3435 (2003).
67. Chow, K. H. *et al.* Intrinsic defects in GaN. I. Ga sublattice defects observed by optical detection of electron paramagnetic resonance. *Phys. Rev. B* **69**, 045207 (2004).
68. Hautakangas, S. *et al.* Direct evidence of impurity decoration of Ga vacancies in GaN from positron annihilation spectroscopy. *Phys. Rev. B* **73**, 193301 (2006).
69. Nykänen, H., Suihkonen, S., Kilanski, L., Sopanen, M. & Tuomisto, F. Low energy electron beam induced vacancy activation in GaN. *Appl. Phys. Lett.* **100**, 122105 (2012).
70. Van de Walle, C. G. Interactions of hydrogen with native defects in GaN. *Phys. Rev. B* **56**, 10020R–10023R (1997).
71. Son, N. T. *et al.* Identification of the gallium vacancyoxygen pair defect in GaN. *Phys. Rev. B* **80**, 153202 (2009).
72. Chichibu, S. F. *et al.* Limiting factors of room-temperature nonradiative photoluminescence lifetime in polar and nonpolar gan studied by time-resolved photoluminescence and slow positron annihilation techniques. *Appl. Phys. Lett.* **86**, 021914 (2005).
73. Lyons, J. L., Janotti, A. & Van de Walle, C. G. Carbon impurities and the yellow luminescence in GaN. *Appl. Phys. Lett.* **97**, 152108 (2010).
74. Maruska, H. P. & Tietjen, J. J. The preparation and properties of vapordeposited singlecrystalline GaN. *Appl. Phys. Lett.* **15**, 327–329 (1969).
75. Ganchenkova, M. G. & Nieminen, R. M. Nitrogen vacancies as major point defects in gallium nitride. *Phys. Rev. Lett.* **96**, 196402 (2006).
76. Yan, Q., Janotti, A., Scheffler, M. & Van de Walle, C. G. Role of nitrogen vacancies in the luminescence of Mg-doped GaN. *Appl. Phys. Lett.* **100**, 142110 (2012).
77. Reshchikov, M. A., Demchenko, D. O., McNamara, J. D., Fernández, S. & Calarco, R. Green luminescence in mg-doped gan. *Phys. Rev. B* **90**, 035207 (2014).
78. Miceli, G. & Pasquarello, A. Self-compensation due to point defects in Mg-doped GaN. *Phys. Rev. B* **93**, 165207 (2016).
79. Buckeridge, J. *et al.* Determination of the nitrogen vacancy as a shallow compensating center in GaN doped with divalent metals. *Phys. Rev. Lett.* **114**, 016405 (2015).
80. Götz, W., Johnson, N. M., Walker, J., Bour, D. P. & Street, R. A. Activation of acceptors in Mg-doped GaN grown by metal-organic chemical vapor deposition. *Appl. Phys. Lett.* **68**, 667–669 (1996).
81. Salviati, G. *et al.* Deep level related yellow luminescence in *p*-type GaN grown by MBE on (0001) sapphire. *Mater. Res. Soc. Proc.* **595**, F99W11.50 (1999).
82. Gelhausen, O., Klein, H. N., Phillips, M. R. & Goldys, E. M. Low-energy electron-beam irradiation and yellow luminescence in activated Mg-doped GaN. *Appl. Phys. Lett.* **83**, 3293–3295 (2003).
83. Kaufmann, U., Schlotter, P., Obloh, H., Köhler, K. & Maier, M. Hole conductivity and compensation in epitaxial GaN:Mg layers. *Phys. Rev. B* **62**, 10867–10872 (2000).
84. Chow, K. H., Watkins, G. D., Usui, A. & Mizuta, M. Detection of interstitial Ga in GaN. *Phys. Rev. Lett.* **85**, 2761–2764 (2000).
85. Limpijumnong, S. & Van de Walle, C. G. Diffusivity of native defects in GaN. *Phys. Rev. B* **69**, 035207 (2004).
86. von Bardeleben, H. J. *et al.* Identification of the nitrogen split interstitial $(N\text{-}N)_N$ in GaN. *Phys. Rev. Lett.* **109**, 206402 (2012).